Biosensors and Bioelectronics 53 (2014) 420–427

Contents lists available at ScienceDirect

Biosensors and Bioelectronics

journal homepage: www.elsevier.com/locate/bios

Direct electrochemistry of myoglobin at reduced graphene oxide-multiwalled carbon nanotubes-platinum nanoparticles nanocomposite and biosensing towards hydrogen peroxide and nitrite

Veerappan Mani [a], Bose Dinesh [b], Shen-Ming Chen [a,*], Ramiah Saraswathi [b,*]

[a] Department of Chemical Engineering and Biotechnology, National Taipei University of Technology, No. 1, Section 3, Chung-Hsiao East Road, Taipei 106, Taiwan, ROC
[b] Department of Materials Science, School of Chemistry, Madurai Kamaraj University, Madurai-625 021, Tamilnadu, India

ARTICLE INFO

Article history:
Received 24 July 2013
Received in revised form
20 September 2013
Accepted 30 September 2013
Available online 18 October 2013

Keywords:
Graphene
MWCNT
Myoglobin
Picomolar
Hydrogen peroxide
Nitrite

ABSTRACT

We described the preparation of a novel nanobiocomposite, reduced graphene oxide- multiwalled carbon nanotubes-platinum nanoparticles/myoglobin (RGO-MWCNT-Pt/Mb) for the direct electrochemistry of myoglobin and its application towards determination of hydrogen peroxide (H_2O_2) and nitrite (NO_2^-). RGO-MWCNT-Pt nanocomposite has been prepared by simple solution based approach and its structure was characterized. RGO-MWCNT-Pt/Mb nanobiocomposite was prepared and attained the direct electrochemistry of Mb with pair of well-defined redox peaks with the formal potential of −0.33 V and peak to peak separation of 22 mV. Amount of electroactive protein (Γ) and heterogeneous electron transfer rate constant (k_s) were calculated to be 1.04×10^{-9} mol cm^{-2} and 9.47 s^{-1}. The sensor displayed lowest detection limit (LOD) of 6 pM which is the lowest LOD ever achieved for the detection of H_2O_2. Two linear ranges were observed for the detection of H_2O_2: (1) 10 pM–0.19 nM with sensitivity of 1.99 ($\pm$0.058) μA pM^{-1} cm^{-2} and (2) 0.25 nM–2.24 μM with sensitivity of 0.037 ($\pm$0.081) μA nM^{-1} cm^{-2}. In addition, the biosensor offered good analytical parameters towards determination of NO_2^- with wide linear range of 1 μM to 12 mM and high sensitivity of 0.1651 ($\pm$0.026) μA μM^{-1} cm^{-2}. The sensor acquires good selectivity, repeatability, reproducibility and stability. The practical feasibility of the sensor has been addressed.

1. Introduction

Graphene, an allotrope of carbon is a two dimensional nanomaterial which is densely arranged in a honeycomb lattice structure with sp^2 hybridized carbon (Novoselov et al., 2004). Graphene based nanocomposite materials find widespread applications, owing to their peculiar physicochemical properties (Soldano et al., 2010). Though graphene can be prepared by number of strategies, chemical method is very attractive method to prepare bulk quantity of graphene via cost effective oxidation-reduction approach (Stankovich et al., 2007). Graphene oxide (GO), oxygenated derivative of graphene is important intermediate and precursor compound in the chemical preparation of graphene and graphene based composite materials, respectively (Dreyer et al., 2010). Inexpensive production from graphite, easy processing in aqueous solutions and available sites for functionalization make GO as a feasible material for the preparation of any kind of new graphene based composite materials (Huang et al., 2012). Interestingly, GO is one of the best dispersant for high level dispersion of CNTs and thereby producing a unique hybrid GO-CNT (Mani et al., 2013). Assembling graphene and CNTs as a hybrid via non covalent $\pi-\pi$ stacking interaction offer great opportunity to collectively harvest the exceptional properties of these two important nanomaterials (Yen et al., 2011). Graphene (or reduced graphene oxide, RGO)–CNT hybrid delivered superior performance over graphene and CNTs and therefore find extensive applications in various research fields (Yen et al., 2011; Deng et al., 2012; Devadas et al., 2012). Recently, our research group reported highly enhanced electrocatalytic performance of RGO-CNT hybrid towards sensor (Unnikrishnan et al., 2012), biosensor (Mani et al., 2013) and biofuel cell applications (Devadas et al., 2012). Owing to the 3D hierarchical arrangement, graphene-CNT hybrid delivered highest edge density per unit normal area compared with all other carbon nanostructures (Stoner and Glass, 2012). On the one hand, CNTs inhibits the restacking of graphene sheets, on the other hand, graphene inhibits the aggregation of individual tubes of CNTs and eventually rendering high stability to the hybrid.

All over the past years, significant efforts were made for the exploitation of carbon nanomaterials as Supporting material to anchor metal nanoparticles (Gopalan et al., 2009; Dey and Raj, 2010). Owing to the large surface area and high stability, graphene-CNT hybrid could be a better Supporting material to anchor the metal

* Corresponding authors. Tel.: +886 227 017 147; fax: +886 227 025 238.
E-mail addresses: smchen78@ms15.hinet.net (S.-M. Chen), saraswathir@yahoo.com (R. Saraswathi).

0956-5663/$ - see front matter © 2013 Elsevier B.V. All rights reserved.
http://dx.doi.org/10.1016/j.bios.2013.09.075

nanoparticles (Rajesh et al., 2013). Therefore, herein we utilized RGO-MWCNT hybrid as a platform for the decoration of Pt nanoparticles via chemical reduction. A previous work pioneered the application of GO as molecular templates of Pt nanoparticle growth and significantly improved biosensor performance was brought by the hybrid nanocomposite owing to the excellent electrocatalytic ability of Pt nanoparticles and unique properties of RGO-CNT hybrid (Shi et al., 2012). In addition with providing good electrocatalytic ability, Pt nanoparticles help to prohibit the aggregation and restacking of graphene sheets and CNTs.

Myoglobin (Mb) a heme protein found in skeletal muscles plays vital role in biological process and therefore it was studied as model system for the electron transfer reactions of heme proteins (Liu and Ju, 2003). Mb exhibited peroxidase-like activity and hence catalytic reaction between Mb and hydrogen peroxide (H_2O_2) was well established in the literature (Carlsen et al., 2003). During the past decades, numerous efforts were made for the exploration of direct electrochemistry of Mb by immobilizing it into various modified electrodes (Yue et al., 2011). Though several CNTs and graphene based modified electrodes were reported for the immobilization of Mb towards determination of H_2O_2, very few offer low detection. In the present work, we report the preparation of a novel nanobiocomposite RGO-MWCNT-Pt/Mb for the direct electron transfer of Mb and determination of H_2O_2. The developed Mb based biosensor achieved low detection limit of 6 pM, which is the lowest LOD achieved for the detection of H_2O_2. Determination of nitrite has profound impact since it is extensively used in food preservation and fertilizing agents. But its excess level has severe health effects and therefore several methods were proposed for the detection of nitrite (Huang et al., 1996). Among all, electrochemical methods are simple and sensitive (Yue et al., 2011). Herein we fabricated Mb immobilized electrochemical biosensor for the sensitive determination of nitrite.

2. Experimental

2.1. Reagents

Myoglobin, graphite, MWCNT were purchased from sigma-Aldrich and used as received. Commercially available contact lens cleaning solution containing 3% H_2O_2 has been acquired from a local drug store in Taipei, Taiwan to demonstrate the practicality of the sensor. All the other reagents used were of analytical grade and used without any further purification. Supporting electrolytes used for the electrochemical studies were 0.1 M Phosphate buffer solutions (PBS), prepared using Na_2HPO_4 and NaH_2PO_4 and the required pH were adjusted either using H_2SO_4 or NaOH. Prior to each experiment, electrolyte solutions were deoxygenated with pre-purified nitrogen for 15 min unless otherwise specified.

Electrochemical measurements were carried out using CHI 611 A work station in a conventional three electrode cell using modified GCE as a working electrode (area 0.071 cm^2), saturated Ag/AgCl as a reference electrode and Pt wire as a counter electrode. Amperometric measurements were performed with analytical rotator AFMSRX (PINE instruments, USA) with a rotating disc glassy carbon electrode (RDGCE) of area 0.21 cm^2. Scanning electron microscopy (SEM) and Transmission electron microscopy (TEM) studies were carried out with Hitachi S-3000H scanning electron microscope and Hitachi H-7000, respectively. Energy-dispersive X-ray (EDX) spectra were recorded using HORIBA EMAX X-ACT (Sensor+24 V=16 W, resolution at 5.9 keV). Powder X-ray diffraction (XRD) studies were performed in a XPERT-PRO (PANalytical B.V., The Netherlands) diffractometer using Cu $K\alpha$ radiation (k=1.54 Å).

2.2. Preparation of RGO-MWCNT-Pt nanocomposite

Schematic representation for the preparation of RGO-MWCNT-Pt/Mb nanobiocomposite is given in Fig. 1. Graphite oxide was prepared from graphite by Hummer's method (Hummers and Offeman, 1958) and exfoliated to GO (1 mg mL^{-1}) via ultrasonication for 1 h. GO was subjected to centrifugation for 30 min (4000 rpm) to remove the unexfoliated graphite oxide. Subsequently CNTs were added to the GO dispersion (1:1 weight ratio) and ultrasonicated for 2 h. Then, the formed GO-CNT hybrid was separated, washed with water, dried overnight and redispersed in water. Afterwards, GO-CNT hybrid was mixed with H_2PtCl_6 and stirred for 30 min. Then HCl was slowly added until pH becomes <2 and then $NaBH_4$ was slowly added with vigorous stirring and

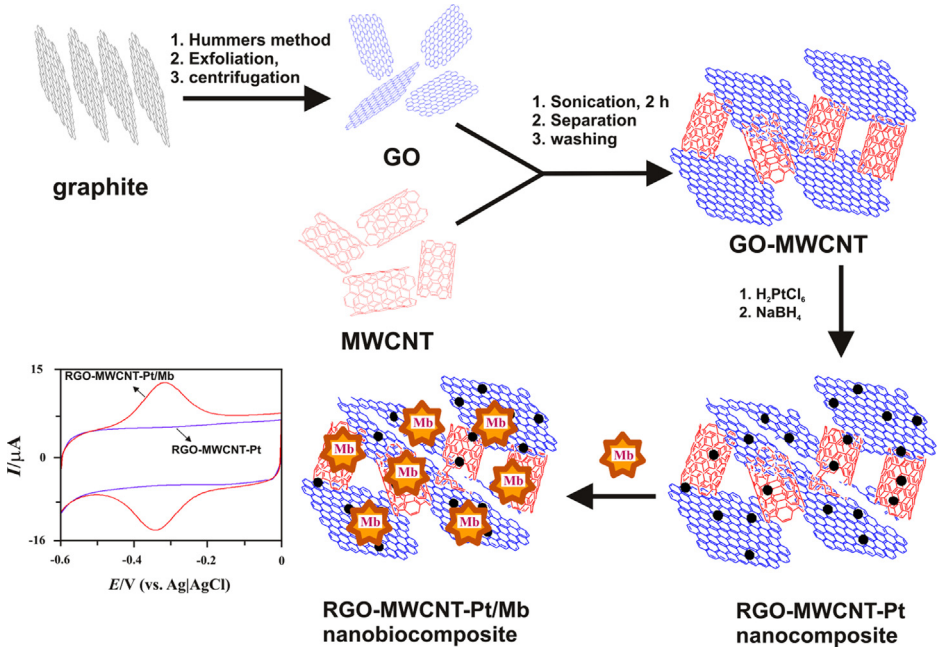

Fig. 1. Schematic representation for the preparation of RGO-MWCNT-Pt/Mb nanobiocomposite. Conditions for CV analysis: CVs were obtained at the respective film modified GCEs in PBS (pH 7) at the scan rate of 50 mV s^{-1}.

the reaction mixture was kept stirring for 12 h. $NaBH_4$ simultaneously reduces the platinum salt into Pt nanoparticles and GO into RGO. Upon completion of reduction, the reaction mixture was centrifuged, washed and overnight dried. Finally, the purified RGO-MWCNT/Pt nanocomposite (1 mg mL^{-1}) was homogeneously dispersed in 0.5% nafion (Nf) and used for the experiments.

2.3. Fabrication of RGO-MWCNT-Pt/Mb nanobiocomposite modified GCE

Prior to electrode modification, the GCE surface (planar and circular surface with an area of 0.071 cm^2) was polished with alumina slurry using a Buehler polishing kit, washed with water, ultrasonicated for 5 min and dried. 40 μL of RGO-MWCNT/Pt nanocomposite dispersion and 60 μL of Mb solution (10 mg mL^{-1} in PBS, pH 7) were mixed and sonicated for 30 min to obtain RGO-MWCNT-Pt/Mb nanobiocomposite. Then 6 μL of the as-prepared RGO-MWCNT-Pt/Mb nanobiocomposite (containing 3.6 μg of Mb) was drop casted onto the pre-cleaned GCE and dried at room temperature. Finally the modified electrode, RGO-MWCNT-Pt/Mb nanobiocomposite modified GCE (RGO-MWCNT-Pt/Mb/GCE) was smoothly washed with water to remove loosely adsorbed Mb. For comparison, MWCNT, RGO and Pt nanoparticles modified GCEs were prepared by adopting the similar procedures.

3. Results and discussions

3.1. Characterization of GO-MWCNT-Pt nanocomposite

3.1.1. SEM and TEM

SEM of GO-MWCNT hybrid (Fig. S1A) exposes the encapsulation of tubular networks of MWCNTs by the GO sheets; this kind of encapsulation of MWCNTs by hydrophilic GO sheets via π–π stacking interactions paves a way for the aqueous dispersion of MWCNTs. TEM of the hybrid (Fig. S1B) also shows the coverage of CNTs by the networks of GO sheets. SEM of the RGO-MWCNT-Pt nanocomposite (Fig. 2A) shows the typical RGO-CNT structure comprising ultrathin RGO sheets, tubes of CNTs with presence of Pt nanoparticles of sizes ranging from 5 to 11 nm. TEM of the nanocomposite (Fig. 2B) also portrays the interconnection of RGO sheets by the tubular networks of MWCNTs with incorporation of Pt nanoparticles, representing a strong affinity between RGO-MWCNT and Pt nanoparticles.

3.1.2. EDX and XRD

Fig. 2 portrays the EDX spectra of GO-MWCNT (C) and RGO-MWCNT-Pt nanobiocomposite (D) films on ITO. EDX spectrum of GO-MWCNT hybrid shows signals for carbon and oxygen with weight percentage of 74.21 and 7.8%, respectively. (Signals related to ITO were

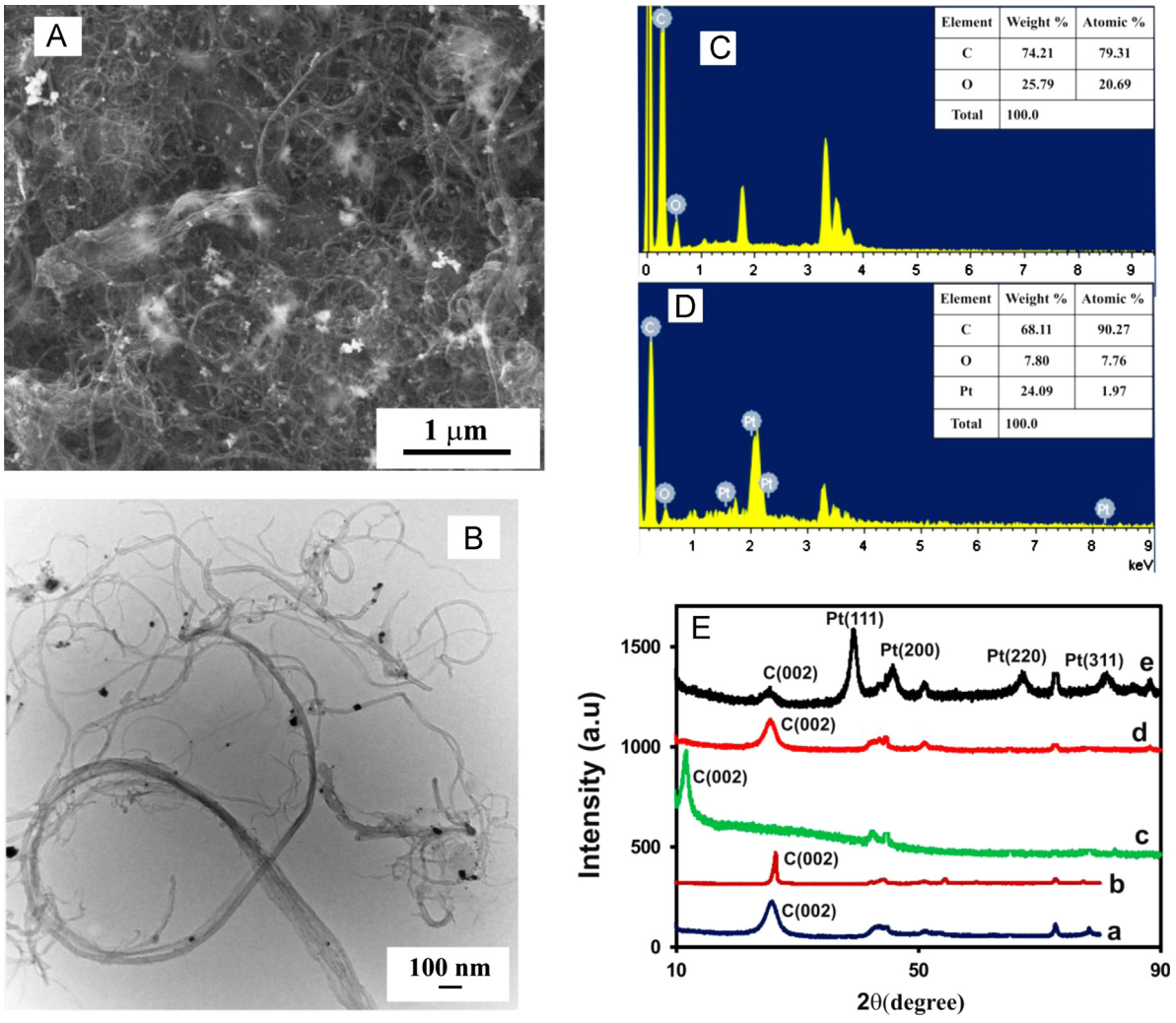

Fig. 2. SEM (A) and TEM (B) images of GO-CNT-Pt nanocomposite. EDX spectra of GO-MWCNT (C) and RGO-MWCNT-Pt nanocomposite (D). XRD patterns (E) of MWCNTs (a), graphite (b), GO (c), GO-MWCNT (d) and RGO-MWCNT-Pt nanocomposite (e).

omitted). EDX spectrum of RGO-MWCNT-Pt nanocomposite portrays the signals of carbon, oxygen and platinum with weight percentage of 68.11, 7.8 and 24.09%, respectively. The existence of Pt signal along with carbon and oxygen proved the formation of Pt nanoparticles onto the hybrid. Moreover decrease in oxygen weight percentage from 20.69 to 7.76, validated the reduction of GO to RGO.

Fig. 2E portrays the XRD patterns of MWCNT (a), graphite (b), GO (c), GO-MWCNT (d) and RGO-MWCNT-Pt nanocomposites (e). XRD patterns of MWCNTs and graphite exhibited a characteristic diffraction peak at 2θ of 26.17 Å (0 0 2), whereas it was completely disappeared in GO with appearance of new diffraction peak at 11.3°, responsible for the large interlayer *d*-spacing (8.02 Å). XRD pattern of GO-MWCNT displays both the above-mentioned peaks, revealed the presence of GO and MWCNTs together as composite. XRD pattern of RGO-CNT-Pt nanocomposite shows the presence of new diffraction peaks at 40.37°, 45.79°, 67.53° and 81.07° ascribed to the fcc crystal structure of Pt nanoparticles. Moreover, disappearance of peak at 11.3° indicates the successful reduction of GO to RGO.

3.2. Surface morphology of RGO-MWCNT-Pt/Mb nanobiocomposite and direct electrochemistry of Mb

SEM image of RGO-MWCNT-Pt/Mb describes the presence of large amount of immobilized Mb (0.0507 mg cm^{-2}) covered onto the porous surface of nanocomposite (Fig. 3A). Large surface area and good affinity of the nanocomposite delivered the entrapment of high amount of Mb. Direct electrochemistry of Mb at various modified electrodes has been investigated by cyclic voltammetry in PBS (pH 7) at the scan rate of 50 mV s^{-1} (Fig. 3B). CV of RGO-MWCNT-Pt/Mb/GCE (curve *d*) exhibited a pair of well defined quasi reversible redox peaks at the formal potential ($E^{0\prime}$) of −0.33 V, which is a characteristic $E^{0\prime}$ of Mb (Fe(III)/Fe(II)). The peak to peak separation (ΔE_p) of the redox couple has been calculated to be 22 mV. Graphene/Mb/GCE (curve *a*) and CNT/Mb/GCE (curve *b*) exhibited feeble redox peaks with much lowered peak currents at $E^{0\prime}$ of −0.38 and −0.37 V, respectively. In addition higher ΔE_p of 41 and 50 mV were observed at the graphene/Mb/GCE and CNT/Mb/GCE, respectively. While only Pt nanoparticles/Mb/GCE (curve *c*) does not exhibited direct electron transfer of Mb. Highly enhanced redox peak currents with very low ΔE_p observed at the RGO-MWCNT-Pt/Mb/GCE than the other film modified electrodes revealed the fast electron electron transfer of Mb at the nanocomposite film.

Fig. 4A shows the CVs of RGO-MWCNT-Pt/Mb/GCE in PBS (pH 7) at different scan rates (ν) from 0.01 to 0.1 V s^{-1}. Good linear relationship observed between the peak currents (I_{pa} and I_{pc}) versus ν proved that the electron transfer is a surface-controlled process. A plot of I_{pa} and I_{pc} versus ν was made (Inset to Fig. 4A) and the corresponding linear regression equations were expressed as, $I_{pa}/\mu A = 69.657\ \nu/V\ s^{-1} - 0.2473$; $R^2 = 0.999$ and $I_{pa}/\mu A = -63.071\ \nu/V\ s^{-1} - 0.1078$; $R^2 = 0.998$. The surface concentration (Γ) of electroactive Mb was calculated to be 1.04×10^{-9} mol cm^{-2}, which is very much larger than the theoretically estimated surface coverage of 1.58×10^{-11} mol cm^{-2} indicated the high loading of Mb. Apparent heterogeneous electron transfer rate constant (k_s) for the direct electron transfer of Mb was calculated to be 9.47 s^{-1} using Laviron (1979) equation.

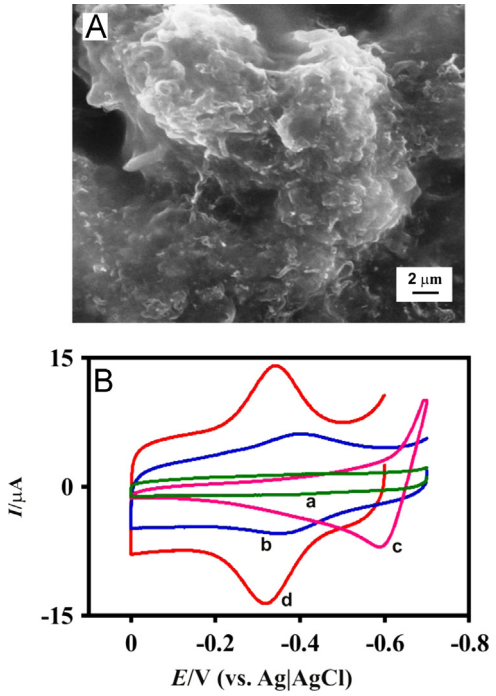

Fig. 3. (A) SEM image of RGO-MWCNT-Pt/Mb nanobiocomposite. (B) CVs obtained at graphene/Mb (a), CNT/Mb (b), Pt nanoparticles/Mb (c) and RGO-MWCNT-Pt/Mb nanobiocomposite (d) modified GCEs in PBS (pH 7) at the scan rate of 50 mV s^{-1}.

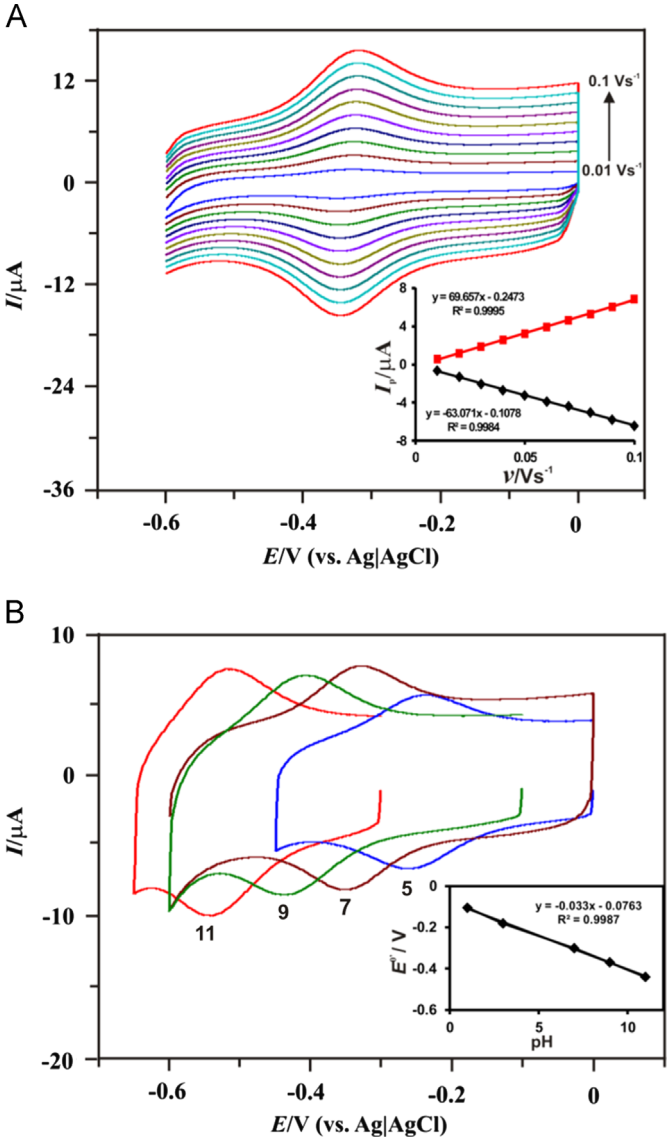

Fig. 4. (A) CVs of RGO-MWCNT-Pt/Mb/GCE in PBS (pH 7) at the scan rates from 0.01 to 0.1 V s^{-1}. Inset: I_{pa} and I_{pc} versus ν. (B) CVs obtained at RGO-MWCNT-Pt/Mb/GCE in various pH solutions (pH 5–11). Inset: pH vs. $E^{0\prime}$.

The estimated k_s value of Mb at RGO-MWCNT-Pt nanobiocomposite is very much higher than the other modified electrodes such as, Single-walled carbon nanohorns (3.50 s^{-1}) (Liu et al., 2010), single-layer graphene nanoplatelet (3.9 s^{-1}) (Yue et al., 2011) and graphene-Pt nanocomposite (0.584 s^{-1}) (Sun et al., 2013). High conductivity and excellent biocompatibility of the nanobiocomposite facilitated such a fast electron shuttling between redox active sites of Mb and electrode surface.

The effect of pH on the direct electrochemistry of Mb has been studied in PBS of various pHs from 5 to 11 at ν of 50 mV s^{-1} (Fig. 4B). The redox couple of Mb retains stable over the entire pH ranges. A negative shift occurs in both oxidation and reduction peak potentials, when pH changes from 1 to 10. Moreover, $E^{0\prime}$ shows linear relationship with different pH values (Inset to Fig. 4B). The linear regression equation was expressed as, $E^{0\prime}$/V= −0.033 (±1.8) pH/(V/pH) −0.076/V; R^2=0.9987. The slope value was 0.033/pH, which is smaller than the theoretical value of 0.057 mV/pH for reversible reactions involving equal number of electrons and protons. This could be attributed to the influence of protonation states of trans ligands close to the heme iron and amino acids around the heme and protonation of water molecules coordinated to the iron center (Sun and Wang, 2007).

3.3. Electrocatalytic activity of RGO-MWCNT-Pt/Mb/GCE towards reduction of H_2O_2

Fig. 5A shows the CVs of RGO-MWCNT-Pt/Mb/GCE in PBS (pH 7) without H_2O_2 (a) and with each addition of 0.1 mM H_2O_2 (b–n; 0.1–1.3 mM). In the absence of H_2O_2, CV of RGO-MWCNT-Pt/Mb/GCE shows characteristic redox peaks of Mb at $E^{0\prime}$ of −0.33 V. The observation of significant increase in I_{pc} upon addition of 0.1 mM H_2O_2 revealed the occurrence of electrocatalytic reduction of H_2O_2. Further increase in the concentration of H_2O_2 leads to linear increase in I_{pc}, whereas I_{pa} was decreased and almost disappeared after some additions. Moreover, a new reduction peak was observed at the potential of −0.155 V ascribed to the reduction of H_2O_2.Thus, RGO-MWCNT-Pt/Mb/GCE exhibited good electrocatalytic ability towards reduction of H_2O_2 and therefore we demonstrated the film as an amperometric sensor for the more sensitive determination. Fig. 5B shows the CVs of RGO-MWCNT-Pt/Mb/GCE in PBS (pH 7) in presence of 1 mM H_2O_2 at various ν from 0.1 to 1 V. The peak currents responsible for the reduction of H_2O_2 were increased linearly from ν of 0.1 to 1 V s^{-1}.

3.4. Amperometric determination of H_2O_2

Fig. 5C, shows the amperometric *i–t* curve obtained at RGO-MWCNT-Pt/Mb/ RDGCE (Rotation speed=1500 RPM) upon sequential addition of 10 pM of H_2O_2 into PBS (pH 7) at regular intervals of 50 s. The applied potential (E_{app}) was hold at −0.35 V. For every addition of H_2O_2, well defined and stable amperometric response was observed. The response currents were increased linearly with the increase in concentrations of H_2O_2 between 10 pM and 0.19 nM (inset a, Fig. 5C). The respective linear regression equation expressed as I_p/μA=0.4186 (±0.071) [H_2O_2]/μA pM^{-1}+5.337 (±1.23); R^2=0.983. Sensitivity has been calculated to be 1.99 (±0.058) μA pM^{-1} cm^{-2}. Detection limit (LOD) was calculated to be 6 pM (RSD at this level was calculated to be 3.54%) using the formula, LOD=3 s_b/S (where, s_b=standard deviation of blank signal and S=sensitivity) (Radoi et al., 2007).

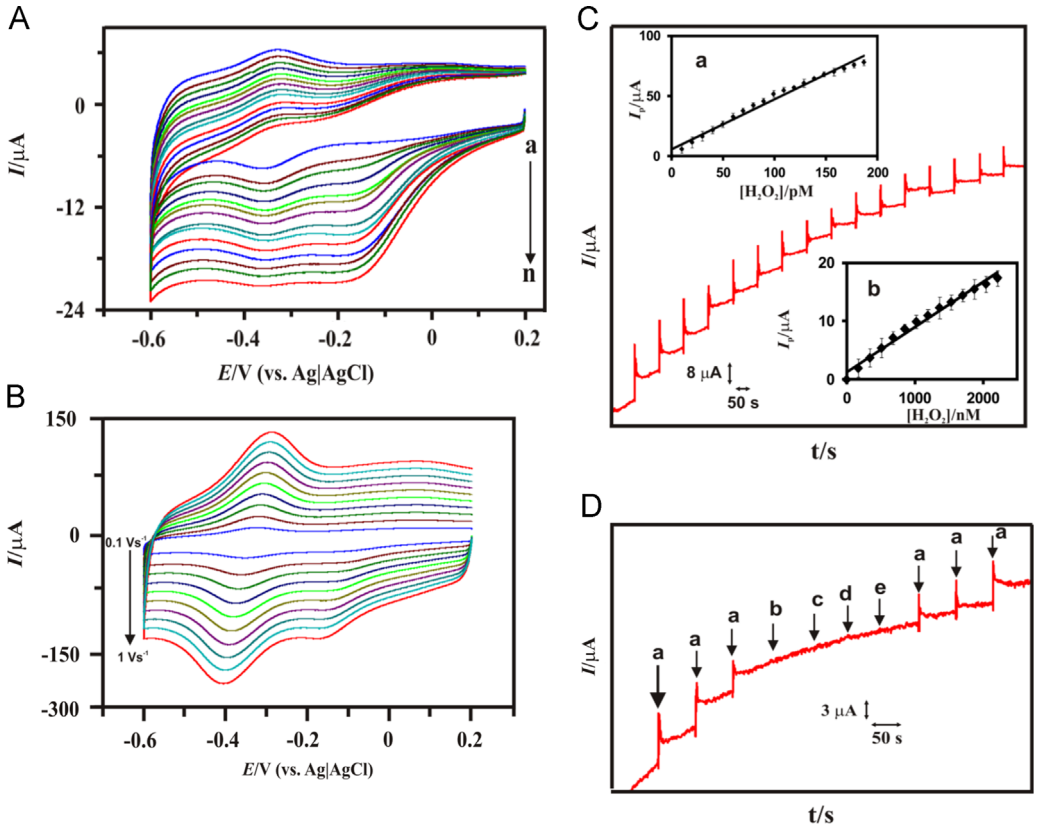

Fig. 5. (A) CVs at RGO-MWCNT-Pt/Mb/GCE in the absence (a) and presence of H_2O_2 (b–n; 0.1–1.3 mM, each successive addition of 0.1 mM) in PBS (pH 7). (B) CVs of RGO-MWCNT-Pt/Mb/GCE in PBS (pH 7) containing 1 mM H_2O_2 at ν from 0.1 to 1 V. (C) Amperometric i–t response at RGO-MWCNT-Pt/Mb/RDGCE upon successive addition of 10 pm H_2O_2 into continuously stirred PBS (pH 7). Rotation rate: 1500 rpm; E_{app}= −0.35 V. Error bars represents standard deviation of three individual measurements. Inset (a): [H_2O_2]/pM vs. I_p/μA. Inset (b): [H_2O_2]/nM vs. I_p/μA. (D) Amperometric response at RGO-MWCNT-Pt/Mb/RDGCE for the successive addition of 1 μM H_2O_2 (a) and each 0.001 μM addition of DA (b), AA (c), UA (d) and glucose (e).

The analytical performance of the proposed sensor towards determination of H_2O_2 is superior over the other reports in terms of wide linear ranges, high sensitivity and lowest LOD (Table S1). Until now the lowest LOD reported for H_2O_2 in the literature were 8 and 10 pM at the chemically activated redox mediator amplex and NAD^+/single walled carbon nanotubes modified electrodes, respectively (Lyon and Stevenson, 2006; Salimi et al., 2008). In this work, we achieved lowest LOD of 6 pM at the RGO-MWCNT-Pt/Mb/GCE with high sensitivity of 1.99 ($\pm$0.058) μA pM^{-1} cm^{-2}. Recently, Woo et al. (2012) reported LOD of 9.4×10^{-6} μM for the detection of H_2O_2 at graphene-CNT hybrid modified electrode. Interestingly, our study shows that incorporation of Mb into graphene-CNT hybrid greatly improves the electrocatalytic performance towards H_2O_2 and offer lowest LOD of 6 pM validating the major role of Mb in the picormolar determination of H_2O_2. The probable reason for this fascinating electrocatalytic behavior of the nanobiocomposite could be due to the perfect combination of exceptional properties of 3D hierarchical RGO-MWCNT hybrid, good electrocatalytic property of Pt nanoparticles and presence of large amount of electroactive Mb.

A second linear range was observed to be wider in the higher concentration of H_2O_2 between 0.25 nM and 2.24 μM (Inset b, Fig. 5C) and the respective linear regression equation can be expressed as: $I_p/\mu A = 0.0077$ ($\pm$0.071) $[H_2O_2]/\mu A\ pM^{-1} + 1.251$ ($\pm$1.23); $R^2 = 0.986$. The sensitivity and LOD at this linear range have been calculated to be 0.037 ($\pm$0.081) μA nM^{-1} cm^{-2} and 0.25 nM. Notably, Sensitivity is relatively lower than that at the lower H_2O_2 concentration (Inset a, Fig. 5C) due to the occurrence of substrate inhibition effects at higher concentration of H_2O_2 (Lyon and Stevenson, 2006).

Selectivity of the sensor towards determination of H_2O_2 has been investigated in the presence of common interfering agents such as dopamine (DA), ascorbic acid (AA), uric acid (UA) and glucose. Fig. 5D shows the amperometric responses of RGO-MWCNT-Pt/Mb/RDGCE for the successive addition of 1 μM of H_2O_2 (a) and 100 fold high concentration (each 1000 μM) of interfering species DA (b), AA (c), UA (d) and glucose (e). Well defined amperometric response was observed towards 1 μM addition of H_2O_2 (a), whereas no noteworthy responses were obtained for the successive addition of 1000 μM of interfering species DA (b), AA (c), UA (d) 1 mM glucose (e). Again well defined amperometric response was observed upon addition of 1 μM H_2O_2 into the same PBS coexisting with the aforementioned interferences. Thus H_2O_2 was selectively detected at the RGO-MWCNT-Pt/Mb/RDGCE even in the coexistence of high concentrations of common interferring species revealed the excellent selectivity of the biosensor.

Practical feasibility of the sensor has been demonstrated in contact lens cleaning solution containing 3% H_2O_2. The required dilutions were made using PBS (pH 7) and amperometry experiments were performed with experiemetal conditions similar to lab sample. RGO-MWCNT-Pt/Mb/RDGCE exhibited well defined amperometric responses towards H_2O_2 in the linear range between 50 pM to and 0.55 nM with sensitivtiy of 0.1985 ($\pm$0.047) μA pM^{-1} cm^{-2}, which shows its appreciable practicality (Fig. S2).

3.5. Electrocatalytic activity of RGO-MWCNT-Pt/Mb/GCE towards NO_2^-

Fig. 6A shows the CVs obtained at the RGO-MWCNT-Pt/Mb/GCE towards absense of NO_2^- (a) and presence of NO_2^- (b–k; 0.1–1 mM). No noticeable catalytic peaks was observed in the absence of nitrite (a), whereas a well defined irreversible anodic peak (I_{pa}) was observed at +0.80 V, upon addition of 0.1 mM nitrite ascribed to the oxidation of nitrite, I_{pa} increased linearly from 0.1 to 1 mM of nitrite (b–k).This could be ascribed to the excellent electrocatalytic performance of the RGO-MWCNT-Pt/GCE towards nitrite oxidation.

The effect of ν on the oxidation of nitrite has been performed at RGO-MWCNT-Pt/Mb/GCE from 0.01 to 0.1 V s^{-1} in PBS (pH 7) towards 1 mM NO_2^-. I_{pa} increased linearly with ν from 0.01 to 0.1 V s^{-1} (Fig. 6B). A linear calibration plot was made between $\nu^{1/2}$ versus I_{pa} and the linear regression equation is expressed as $I_{pa}/\mu A = 35.044\ \nu^{1/2}/(V\ s^{-1})^{1/2} + 4.246$; $R^2 = 0.989$ (inset to Fig. 6B). Good linear relationship obtained between $\nu^{1/2}$ and I_{pa} revealed that the oxidation process is a diffusion controlled process. Remarkably, the nitrite oxidation is a second-order homogeneous disporportionation process and the mechanism of the oxidation can be expressed as eq. (1) (Guidelli et al., 1972).

$$NO_2^- + H_2O \rightarrow NO_3^- + 2H^+ + 2e^- \quad (1)$$

3.6. Amperometric determination of nitrite

Fig. 6C shows the amperometric *i–t* curve obtained at RGO-MWCNT-Pt/Mb/RDGCE upon each successive addition of 1 μM nitrite into PBS (pH 7). The electrode was rotated at a speed of 1500 RPM and the applied potential (E_{app}) was hold at +0.8 V. Well defined and fast amperometric response was observed for the each addition of nitrite in the linear range of 1 μm to 12 mM. A calibration plot was made between [nitrite] versus I_p (inset to Fig. 6C). The respective linear regression equation was expressed as $I_p/\mu A = 0.0347$ ($\pm$0.011) $[NO_2^-]/\mu A\ \mu M^{-1} + 19.40$ ($\pm$1.074), $R^2 = 0.994$. LOD and sensitivity were calculated to be 0.93 μM and 0.1651 ($\pm$0.026) μA μM^{-1} cm^{-2}. The important analytical parameters such as linear range, sensitivity and LOD of the sensor were compared with previous reports (Table S2).

Interference experiments were performed to investigate the selectivity of the proposed sensor towards detection of NO_2^- in presence of common ions such as NH_4Cl, NaF, KCl, NaCl, glucose and nitrate (Fig. 6D), RGO-MWCNT-Pt/Mb/RDGCE exhibited well defined amperometric response towards detection of 30 μM of nitrite (a), whereas no noteworthy amperometric responses were observed for the addition of 170, 170, 150, 150, 300 and 160 fold excess of NH_4Cl (b), NaF (c), KCl (d), NaCl (e), glucose (f) and nitrate (g), respectively. But quick and stable response was observed again for the addition of 30 μM nitrite into the same PBS coexisting with the abovesaid interferences. Thus RGO-MWCNT-Pt/Mb/RDGCE selectively detects nitrite even in the presence of high concentrations of common interferring species.

Practicality of the sensor has been demonstrated by the determinaion of NO_2^- in various water samples collected from different water sources such as rain, river and tap. Known amounts of NO_2^- were spiked into the water samples and analyzed using RGO-MWCNT-Pt/Mb/RDGCE. The added and found values showed good recoveries from 96.6 to 103.4% (via standard addition method) revealed the appreciable practicality of the proposed sensor (Table S3).

3.7. Stability, repeatability and reproducibility studies

The redox peak currents of the RGO-MWCNT-Pt/Mb/GCE have been monitored to investigate the stroage stability of the sensor. A 94.6% of the initial peak currents were retained even after one month of electrode storage at 4 °C in refrigerator validated good storage stability of the sensor. The sensor exhibited related standard deviation (RSD) of 3.68 and 3.29% for the five repetitive measurements at the same modified electrode (repeatability) and for the five different measurments at five different electrodes (reproducibility) towards determination of 3 μM of NO_2^- via amperometry. Likewise, the sensor exhibited R.S.D of 4.58 and 4.16% for the repeatability and reproducibility of five measurments

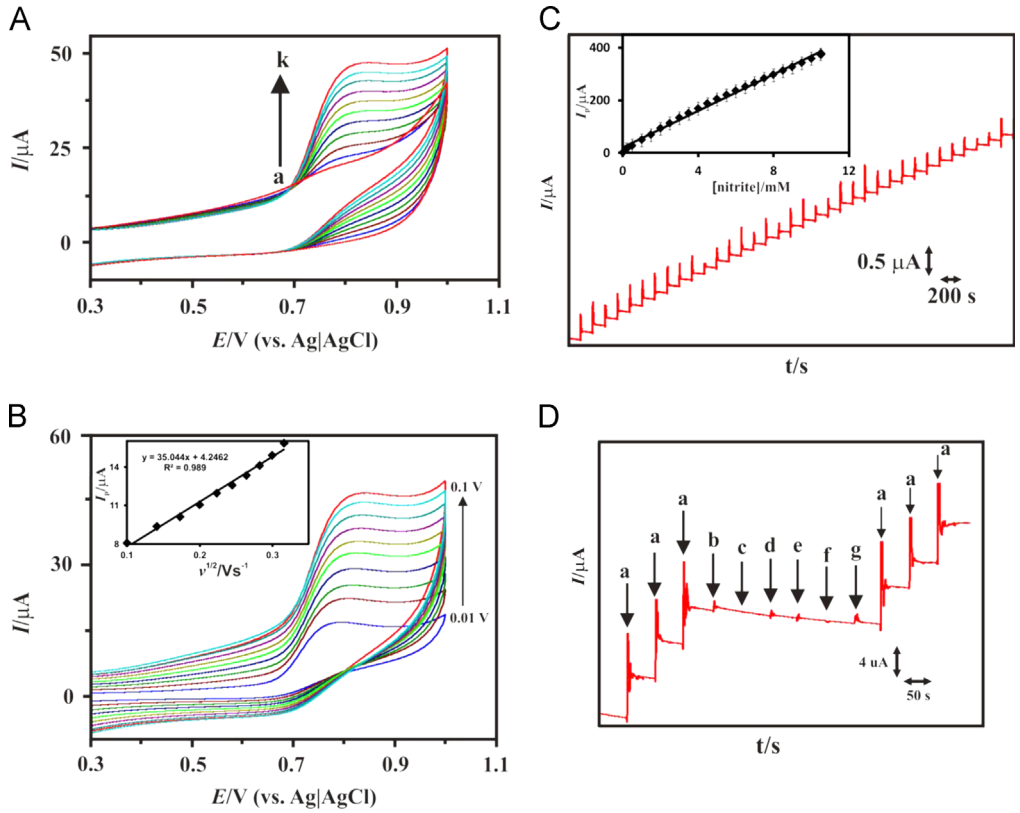

Fig. 6. (A) CVs at RGO-MWCNT-Pt/Mb/GCE without NO_2^- (a) and with each addition of 0.1 mM NO_2^- (a–k; 0.1–1 mM) in PBS (pH 7). (B) CVs of RGO-MWCNT-Pt/Mb/GCE in PBS (pH 7) containing 1 mM nitrite at ν from 0.01 to 0.1 V. Inset: $\nu^{1/2}$ vs. I_{pa}. (C) Amperometric i–t response obtained at RGO-MWCNT-Pt/Mb/RDGCE upon successive addition of 1 μM nitrite into PBS (pH 7). Rotation rate: 1500 rpm; $E_{app} = +0.8$ V. Inset: [nitrite] vs. I_p. Error bars represents standard deviation of three individual experiments. (D) Amperometric responses at RGO-MWCNT-Pt/Mb/RDGCE for the successive addition of 30 μM nitrite (a) and 170, 170, 150, 150, 300 and 160 fold excess of NH_4Cl (b), NaF (c), KCl (d), NaCl (e), glucose (f) and nitrate (g), respectively.

towards determination of 10 pM of H_2O_2 via amperometry. The satisfactory RSD values obtained at the composite film modified electrode validated the good repeatability and reproduciablity towards determination of nitrite and H_2O_2.

4. Conclusions

In summary, we prepared a novel nanobiocomposite, RGO-MWCNT-Pt/Mb and characterized by SEM, EDX, TEM and XRD techniques. Direct electrochemisty of Mb was observed with highly enhanced peak currents and low ΔE_p. The fabricated biosensor detects H_2O_2 in picomolar level and achieved lowest LOD of 6 pM. In addition the biosensor exhibited excellent electrocatalytic ability towards determination of NO_2^- with wide linear range of 1 μm–12 mM and low LOD of 0.93 μM. The biosensor acquires good selectivity, repeatability, reproducibility, stability and practicality. Exceptional properties of the nanocomposite such as three dimensional hierarchical arrangement, large surface area, high conductivity, long term stability, outstanding electrocatalytic, and anti-interference abilities give great hope for the immobilization of other redox proteins or enzymes for the biosensor applications.

Novelty statement

- A novel nanobiocomposite reduced graphene oxide-multiwalled carbon nanotubes-platinum nanoparticles/myoglobin (RGO-MWCNT-Pt/Mb) has been prepared and characterized.
- Fast direct electrochemistry of myoglobin (Mb) has been attained with very low peak to peak separation of 22 mV and high rate constant (k_s) of 9.47 s^{-1}.
- RGO-MWCNT-Pt/Mb nanobiocomposite modified electrode exhibited lowest detection limit (LOD) of 6 pM with high sensitivity of 1.99 ($\pm$0.058) μA pM^{-1} cm^{-2} towards determination of H_2O_2. Until now the lowest LOD reported for H_2O_2 in the literature were 8 and 10 pM at the chemically activated redox mediator amplex and NAD^+/single walled carbon nanotubes modified electrodes, respectively. In this work, we achieved very lowest LOD of 6 pM at the RGO-MWCNT-Pt/Mb/GCE with high sensitivity. To best of our knowledge this is the lowest LOD ever achieved for the detection of H_2O_2.
- The sensor also exhibited excellent analytical parameters towards amperometric determination of nitrite with wide linear range of 1 μM–12 mM and high sensitivity of 0.1651 ($\pm$0.026) μA μM^{-1} cm^{-2}.

Acknowledgement

This work was supported by the National Science Council and the Ministry of Education of Taiwan (Republic of China). The National Science Council of Taiwan and Department of Science and Technology, India under Indo-Taiwan Science and Technology Program are gratefully acknowledged. Bose Dinesh gratefully acknowledges the University Grants Commission for a meritorious Fellowship.

Appendix A. Supplementary material

Supplementary data associated with this article can be found in the online version at http://dx.doi.org/10.1016/j.bios.2013.09.075.

References

Carlsen, C.U., Skovgaard, I.M., Skibsted, L.H., 2003. J. Agric. Food Chem. 51, 5815–5823.
Deng, J.-H., Zheng, R.-T., Zhao, Y., Cheng, G.-A., 2012. ACS Nano. 6, 3727–3733.
Devadas, B., Mani, V., Chen, S.-M., 2012. Int. J. Electrochem. Sci. 7, 8064–8075.
Dey, R.S., Raj, C.R., 2010. J. Phys. Chem. C 114, 21427–21433.
Dreyer, D.R., Park, S., Bielawski, C.W., Ruoff, R.S., 2010. Chem. Soc. Rev. 39, 228–240.
Gopalan, A.I., Lee, K.-P., Ragupathy, D., 2009. Biosens. Bioelectron. 24, 211–2217.
Guidelli, R., Pergola, F., Raspi, G., 1972. Anal. Chem. 44, 745–755.
Huang, Y., Yan, W., Xu, Y., Huang, L., Chen, Y., 2012. Macromol. Chem. Phys. 213, 1101–1106.
Huang, Y.G., Ji, J.D., Hou, Q.N., 1996. Mutat. Res. Fund. Mol. Mech. Mut. 358, 7–14.
Hummers, W.S., Offeman, R.E., 1958. J. Am. Chem. Soc. 80, 1339.
Laviron, E., 1979. J. Electroanal. Chem. 101, 19–28.
Liu, S., Ju, H., 2003. Electroanalysis 15, 1488–1493.
Liu, X., Li, H., Wang, F., Zhu, S., Wang, Y., Xu, G., 2010. Biosens. Bioelectron. 25, 2194–2199.
Lyon, J.L., Stevenson, K.J., 2006. Anal. Chem. 78, 8518–8525.
Mani, V., Devadas, B., Chen, S.-M., 2013. Biosens. Bioelectron. 41, 309–315.
Novoselov, K.S., Geim, A.K., Morozov, S.V., Jiang, D., Zhang, Y., Dubonos, S.V., Grigorieva, I.V., Firsov, A.A., 2004. Science 306, 666–669.
Radoi, A., Compagnone, D., Devic, E., Palleschi, G., 2007. Sens. Actuators, B 121, 501–506.
Rajesh, Paul, Mulchandani, A., R.K., 2013. J. Power Sources 223, 23–29.
Salimi, A., Miranzadeh, L., Hallaj, R., Mamkhezri, H., 2008. Electroanalysis 20, 1760–1768.
Shi, J., Zhang, H., Snyder, A., Wang, M.-x., Xie, J., Porterfield, D.M., Stanciu, L.A., 2012. Biosens. Bioelectron. 38, 314–320.
Soldano, C., Mahmood, A., Dujardin, E., 2010. Carbon 48, 2127–2150.
Stankovich, S., Dikin, D.A., Piner, R.D., Kohlhaas, K.A., Kleinhammes, A., Jia, Y., Wu, Y., Nguyen, S.T., Ruoff, R.S., 2007. Carbon 45, 1558–1565.
Stoner, B.R., Glass, J.T., 2012. Diamond Relat. Mater. 23, 130–134.
Sun, W., Li, L., Lei, B., Li, T., Ju, X., Wang, X., Li, G., Sun, Z., 2013. Mater. Sci. Eng., C 33, 1907–1913.
Sun, Y.-X., Wang, S.-F., 2007. Bioelectrochemistry 71, 172–179.
Unnikrishnan, B., Mani, V., Chen, S.-M., 2012. Sens. Actuators, B 173, 274–280.
Woo, S., Kim, Y.-R., Chung, T.D., Piao, Y., Kim, H., 2012. Electrochim. Acta 59, 509–514.
Yen, M.-Y., Hsiao, M-C., Liao, S.-H., Liu, P.-I., Tsai, H.-M., Ma, C.-C.M., Pu, N.-W., Ger, M.-D., 2011. Carbon 49, 3597–3606.
Yue, R., Lu, Q., Zhou, Y., 2011. Biosens. Bioelectron. 26, 4436–4441.